Impact of Annealing and Doping on the Structural and Optical Characteristics of Copper Oxide Nanopowders Synthesized by Solgel Method

R. Bacha[1]*, A. Chaieb[1], A. L. Bouchetout[1], S. Chala[2], Y. Naoui[3]

[1]Laboratory of crystallography, Physics Department, University of Constantine 1, 25000, Constantine, Algeria.
[2]Institute of Electrical and Electronic Engineering, University of M'Hamed Bougara, 35000, Boumerdes, Algeria.
[3]Laboratory of Thermodynamics and Surfaces Treatment of Materials, Physics Department, University of Constantine 1, 25000, Constantine, Algeria.

***ABSTRACT*:** Copper oxide (CuO) is a promising p-type semiconductor for catalysis, solar cells, and gas sensors. Doping with zinc oxide (ZnO) can further modify its structural and optical properties. However, the combined effects of annealing temperature and ZnO doping concentration on the structural and optical characteristics of CuO nanopowders synthesized via the sol–gel method remain insufficiently understood. This study aims to synthesize pure and ZnO-doped CuO nanopowders and to investigate the impact of annealing and doping on their crystallite size, phase composition, and optical band gap. Pure CuO nanopowders were prepared by a sol–gel precipitation method using copper chloride dihydrate ($CuCl_2 \cdot 2H_2O$) as precursor, with sodium hydroxide added dropwise at 100 °C. Pure ZnO nanopowders were separately synthesized from zinc acetate. Doped CuO/ZnO powders with ZnO concentrations of 0.2%, 0.4%, 0.6%, 0.8%, 7%, and 10% were obtained by mechanical blending and grinding, followed by annealing at 450 °C or 750 °C. Structural properties were characterized by X-ray diffraction (XRD), scanning electron microscopy (SEM), and Fourier-transform infrared spectroscopy (FTIR). Optical properties were analyzed using UV-visible spectrophotometry, and band gaps were determined via the second derivative and Tauc-Lorentz methods. XRD confirmed a monoclinic CuO phase (C2/c) with lattice parameters a = 4.685 Å, b = 3 Å, c = 5.132 Å, β = 99.52°. Crystallite size increased from 10.92 nm (unannealed) to 14.18 nm (450 °C) for pure CuO, and from 15.23 nm (0% ZnO) to 17.51 nm (0.8% ZnO). The optical band gap of pure CuO was 3.89 eV, a ~2.7 eV blue shift from bulk CuO. The sol–gel method with controlled annealing and doping effectively tailors the structural and optical properties of CuO nanopowders, making them suitable for future applications such as heterogeneous catalysis and optoelectronic devices.

***KEYWORDS*:** Annealing, Copper Oxide, Optical properties, Nanopowders, Sol-gel, X-ray diffraction.

[Received: Oct. 03, 2025; Revised: Jan. 01, 2026; Accepted: Feb. 16, 2026] Print ISSN: 0189-9546 | Online ISSN: 2437-2110

I. INTRODUCTION

Recently, there has been a noticeable increase in research efforts aimed at discovering new materials suitable for various applications across different fields. Besides composition and structure, size has emerged as a fundamental parameter that can be manipulated to enhance performance.

Due to progress in nanotechnology and its numerous possibilities, the synthesis of metal oxide nanostructures has garnered significant attention, mainly because of their fundamental qualities and wide range of technological uses (García et al., 2020; Wang et al., 2020; Aldeen et al., 2020; Maache et al., 2020). Copper oxide (CuO), having a narrow band gap of 1.2 eV, appears as an important p-type semiconductor, making it highly valuable for diverse practical uses. Additionally, the structural stability and diversity of metal oxides make them currently regarded as the most promising supports for heterogeneous catalysts. Due to its narrow band gap, high catalytic activity, non-toxic nature, and affordable price, CuO is used as a catalyst detector and in various heterogeneous catalysts. Moreover, it is used as a catalyst for the water-gas shift reaction (Kumar et al., 2007; Swastika et al., 2019; Dasireddy et al., 2020), lithium batteries (Xu et al., 2019; Cao et al., 2019; Verrelli et al., 2013), magnetic phase transitions (Sukhorukov et al., 1998; Wang et al., 2016), high-transition temperature superconductors (Li et al., 2019; Yip et al., 1992), solar cells (Lam et al., 2020), and nanofluids (Nikkhah et al., 2015; Zhu et al., 2011).

Another metallic oxide is zinc oxide (ZnO). It is an n-type semiconductor with a direct wide band gap of 3.3 eV and a large exciton binding energy of 60 meV (Chala et al., 2022; Mursal et al., 2018). It is used in various technological and industrial fields such as anti-corrosion, anti-bacteria, and the elimination of phenol from synthetic and pharmaceutical wastewater (Sridar et al., 2018; Kahsay, 2021; Akpomie et al., 2021), as well as in photocatalysts (Chen et al., 2017; Widiyandari et al., 2018; Noman et al., 2021), optoelectronic and solar cell devices (Elbar et al., 2021; Chala et al., 2018; Taouririt et al., 2019; Jang et al., 2019; Shaheera et al., 2020; Ghalmi et al., 2022), and gas detectors (Kang et al., 2021; Sonker et al., 2015; Agarwal et al., 2019).

The doping of CuO with ZnO, or the formation of nanocomposites that produce a mixture of two semiconductors, reveals new physical and optical properties and changes the optical band gap value, where an increase in ZnO ratio causes an

*Corresponding author: rabie.bacha@doc.umc.edu.dz

doi: http://doi.org/10.63746/njtd.v23i1.4067

increase in the band gap energy. The quantum size effect of semiconductors also contributes to the increase in the band gap (Yathisha et al., 2018; Ashwani et al., 2017).

Extensive research has been conducted on copper oxide nanoparticles doped with ZnO, or CuO/ZnO nanocomposites, primarily due to their significant application potential and the emergence of new properties. These nanocomposites exhibit enhanced optical, electrical, and magnetic properties compared to pure CuO, making them a subject of intense investigation. Among these applications are light-emitting diodes (LEDs) (Khadar, 2019; Jamali et al., 2009; Kim et al., 2008), photocatalytic activity (Lavín et al., 2019; Rahemi et al., 2018), antibacterial activity (Jan et al., 2019; Bandekar et al., 2020), and humidity sensing (Zhang et al., 2009; Thiwawong et al., 2018).

Various methods for the synthesis of copper oxide nanoparticles doped with ZnO and CuO/ZnO nanocomposites have been used in many studies, such as hydrothermal, co-precipitation, and ultrasonic spray methods.

Synthesizing and characterizing CuO nanopowders, and studying the impact of heat treatment and doping on crystallite size, structure, and optical properties, were the objectives of this study.

II. MATERIALS AND METHODS

A. Synthesis of Pure CuO Nanopowders

A precursor solution of copper chloride dihydrate ($CuCl_2 \cdot 2H_2O$) was prepared by dissolving 1.7 g of the solid powder in 50 mL of distilled water. The solution was agitated at ambient temperature for 5 minutes to obtain a homogeneous solution with a concentration of 0.2 mol/L. Separately, a sodium hydroxide (NaOH) solution was prepared by dissolving 1.6 g of NaOH powder in 50 mL of distilled water at ambient temperature, yielding a concentration of 0.8 mol/L.

To synthesize CuO nanopowder, 50 mL of the copper chloride solution (0.2 M) was placed in a beaker, and 1 mL of acetic acid (CH_3COOH) was added. The mixture was heated to 100 °C under magnetic stirring for 30 minutes. During heating, the NaOH solution (0.8 M) was added dropwise. A gradual color change was observed, along with the appearance of a dark green color, which eventually turned into a black precipitate, indicating the formation of copper oxide. The resulting compound was dried in air for several days, yielding a black polycrystalline powder.

B. Synthesis of Pure ZnO Nanopowders

To prepare ZnO nanopowder, 45.5 g of hydrogenated zinc acetate was dissolved in 250 mL of distilled water. The solution was heated to 80 °C with magnetic stirring to obtain a homogeneous solution. The NaOH solution was then added dropwise under magnetic stirring until a white precipitate (gel) appeared. The gel was left in air for ten days to obtain a white powder, which was then ground and annealed for two hours to obtain nanometric pure ZnO powder.

C. Synthesis of ZnO-Doped CuO Nanopowders

To obtain CuO doped with ZnO nanopowders, calculated masses of pure ZnO and pure CuO powder were blended and ground to ensure a homogeneous mixture and good crystallization. Atomic doping percentages of 0.2%, 0.4%, 0.6%, 0.8%, 7%, and 10% ZnO were prepared. Each mixture was annealed at 450 °C or 750 °C for 2 hours to simultaneously promote crystallization and doping.

D. Characterization Techniques

1) X-ray diffraction (XRD)

The crystal structure, lattice parameters, and grain size of the prepared powders were confirmed using a Bruker D8 Advance diffractometer with a copper anticathode ($\lambda CuK\alpha = 1.5406$ Å) as the X-ray source. The generator was operated at 22 kV and 15 A, with a step size of 0.05°. Diffraction spectra were recorded in the 2θ range of 6° to 100°.

2) Fourier-transform infrared spectroscopy (FTIR)

FTIR spectra of pure CuO powder samples were recorded using a Shimadzu FTIR-8400-S spectrometer in the spectral range of 400–4000 cm^{-1}.

3) Scanning electron microscopy (SEM) and energy-dispersive X-ray spectroscopy (EDX)

The morphology and chemical composition of the produced samples were examined using a Jeol JSM-7001F scanning electron microscope equipped with an EDX unit.

4) UV-visible spectrophotometry

Optical properties were analyzed using a PerkinElmer Lambda 19 double-beam spectrophotometer over a wavelength range of 190 nm to 3200 nm.

E. Grain Size Analysis

The Debye–Scherrer formula (Equation 1) was used to determine the grain size:

$$D = K\lambda / \beta \cos\theta \quad (1)$$

where θ is the diffraction angle, β is the full width at half maximum (FWHM) of the peak, λ is the X-ray wavelength, and K is the Scherrer constant. The first three most intense peaks corresponding to the planes (002), (111), and (-202) were used for calculation.

IV. RESULTS AND DISCUSSION

A. Structural characterization

1) XRD Analysis

i. Effect of annealing temperature on pure CuO

The XRD patterns of pure CuO powders exposed to different annealing temperatures (unannealed, 100 °C, and 450 °C) are shown in Figure 1. Well-defined peaks in the diffraction patterns indicate that the CuO compound crystallized with high quality. The patterns allowed identification of a monoclinic phase with space group symmetry C2/c and specific lattice parameters: a = 4.685 Å, b = 3 Å, c = 5.132 Å, and $\beta = 99.52°$. Compared to ASTM No. 41-0254 data, the first three prominent peaks observed at $2\theta = 35.52°$, 38°, and 68° correspond to the diffraction planes (-202), (-111, 002), and (111, 200), respectively, for powders annealed at 450 °C and 100 °C.

For the unannealed powder, a slight difference in the diffraction peaks at lower angles was observed, along with an increase in the intensity of the three main peaks at $2\theta = 35.27°$, 38°, 48.63°, and 55°, corresponding to the same planes: (-202), (-111, 002), and (111, 200). All observed peaks align with the monoclinic phase of CuO, indicating that the prepared powder is pure and devoid of any other phases or impurities such as Cu_2O or $Cu(OH)_2$, highlighting the material's structural stability under heat treatment. Furthermore, all peaks exhibited broadening, indicating small crystallite sizes. The XRD peak intensity increases with increasing annealing temperature, accompanied by a decrease in the full width at half maximum (FWHM),

suggesting recrystallization and crystallite growth in specific directions as annealing temperature rises (Parmigiani et al., 1988).

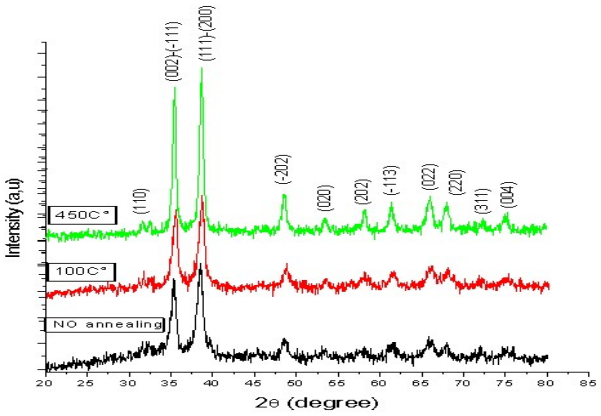

Figure 1 XRD patterns of CuO powders at different annealing temperatures

ii. Effect of annealing temperature on doped CuO/ZnO (constant 7% ZnO)

Figures 2 and 3 show a comparison of the XRD patterns of CuO doped with 7% ZnO at annealing temperatures of 450 °C and 750 °C, respectively. As annealing temperature increased from 450 °C to 750 °C, new peaks corresponding to ZnO appeared. At 750 °C, eight ZnO peaks were observed, whereas only two ZnO peaks were present at 450 °C. The peak widths narrowed with increasing temperature due to increased crystallite size. The improved peak resolution indicates good crystallite quality in the elaborated materials.

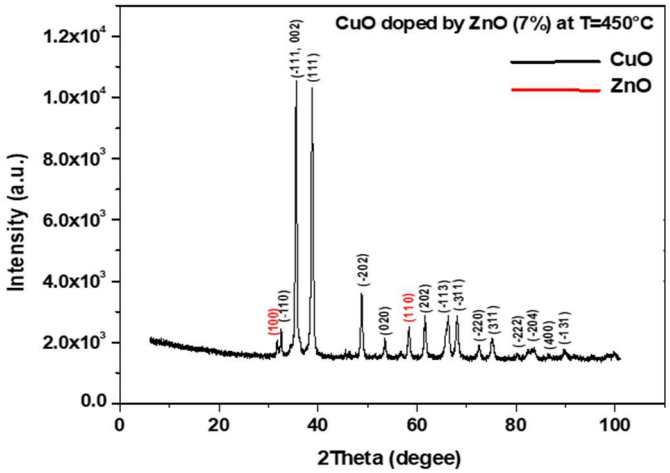

Figure 2 XRD pattern of CuO powder doped by 7% ZnO at annealing temperature of 450°C

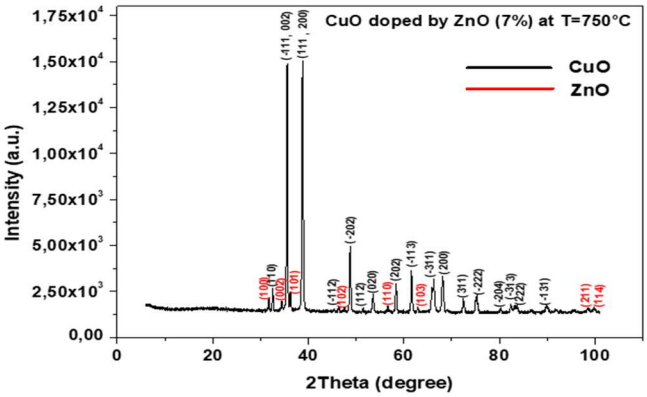

Figure 3 XRD pattern of CuO powder doped by 7% ZnO at annealing temperature of 750°C

iii. Effect of annealing temperature on doped CuO/ZnO (constant 10% ZnO)

Figures 4 and 5 show XRD patterns of CuO doped with 10% ZnO at annealing temperatures of 450 °C and 750 °C, respectively. Similar trends were observed: higher annealing temperature produced more ZnO peaks and sharper diffraction lines.

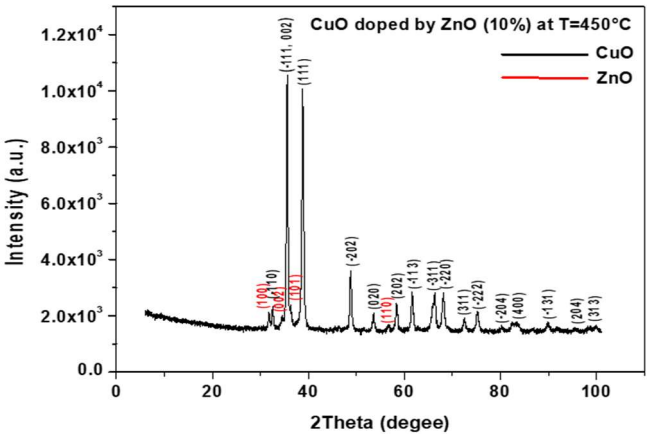

Figure 4 XRD pattern of CuO powder doped by 10% ZnO at annealing temperature of 450°C

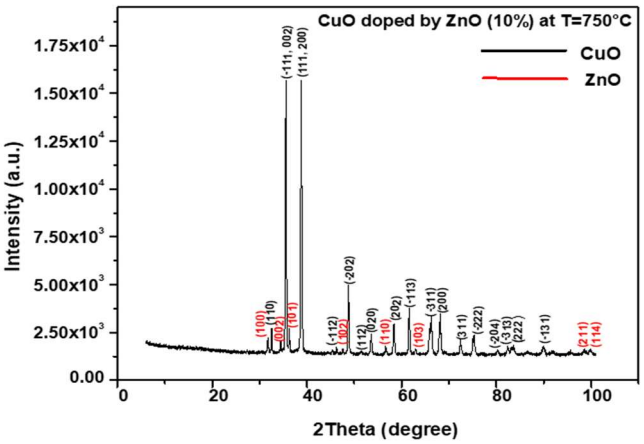

Figure 5 XRD pattern of CuO powder doped by 10% ZnO at annealing temperature of 750°C

iv. Effect of doping concentration at constant annealing temperature

At an annealing temperature of 450 °C, the 7% ZnO-doped sample exhibited two ZnO peaks, while the 10% ZnO-doped sample exhibited four ZnO peaks. At 750 °C, both doping concentrations showed similar spectral patterns, although a slight shift in 2θ positions was observed. Comparing the XRD spectrum of CuO doped with 10% ZnO and annealed at 750 °C with ASTM data No. 05-0664 for wurtzite-structured (hexagonal) ZnO, three prominent peaks were observed at 2θ = 31.75° (100 plane), 34.46° (002 plane), and 36.26° (101 plane). The presence of these ZnO diffraction peaks in the nanocomposites further confirms the formation of CuO/ZnO nanocomposites.

v. Effect of low doping concentrations (0.2–0.8% ZnO) at 450 °C

Figure 6 shows typical XRD patterns of pure CuO and ZnO-doped CuO nanopowders at different doping ratios (0.2%, 0.4%, 0.6%, and 0.8%) annealed at 450 °C. All peaks were indexed to the monoclinic phase of CuO with space group C2/c, consistent with ASTM file No. 41-0254. The main peaks at 2θ = 35.43°, 38.63°, and 48.60° correspond to the diffraction planes (002), (111), and (-202), respectively, as characteristic peaks for the monoclinic phase of pure CuO nanopowders. No impurities such as Zn or Cu_2O were detected in the XRD patterns. The sharpness of the diffraction peaks indicates the formation of highly crystalline, single-phase CuO nanopowders doped with ZnO. This result shows that substitution of Cu^{2+} ions by Zn^{2+} ions in the CuO system did not distort the crystal structure of the base CuO matrix.

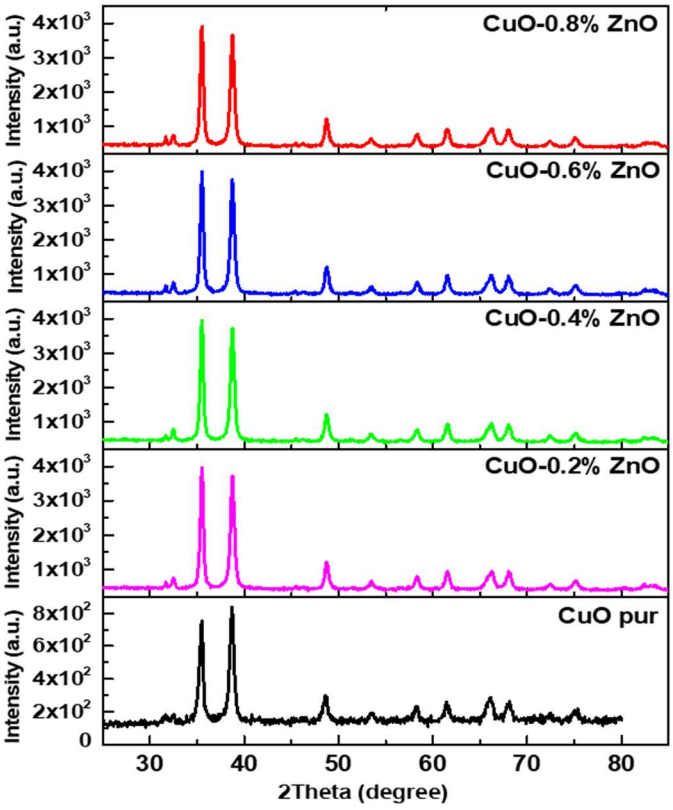

Figure 6 XRD patterns of CuO doped ZnO nano powders at different doping ratios

B. Effect of annealing temperature on pure CuO grain size

Table 1 presents the grain size values for pure CuO powders at different annealing temperatures. The crystallite sizes range from 10.92 nm to 14.18 nm, confirming the nanometric size of the material. Figure 7 shows the effect of annealing temperature on crystal size, revealing a linear, directly proportional relationship.

Table 1 Grain size of pure CuO crystallites

Sample	Orientation	Grain size (nm)
CuO without annealing	(111, 200)	10.92
CuO annealed at 100 °C	(111, 200)	11.83
CuO annealed at 450 °C	(111, 200)	14.18

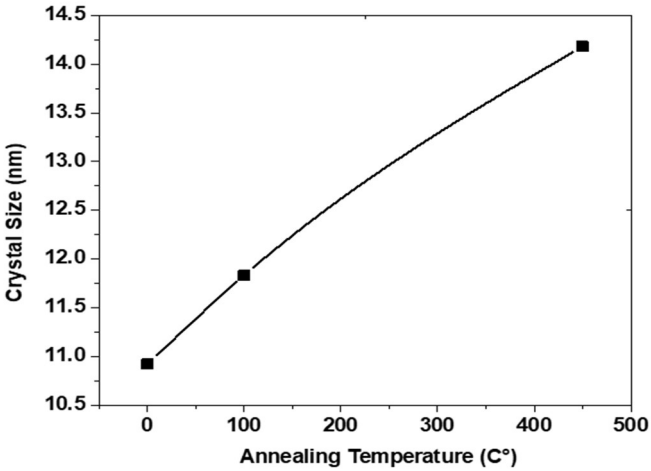

Figure 7 Grain size as a function of annealing temperature

vi. Effect of doping concentration on grain size (0–0.8% ZnO at 450 °C)

Table 2 presents the crystallite sizes for CuO doped with different ZnO concentrations (0%, 0.2%, 0.4%, 0.6%, and 0.8%) and annealed at 450 °C.

Table 2 Grain size for CuO doped with ZnO powders at different ratios

Zn (%)	2θ°	Relative intensity (%)	D (nm)	Average Grain size (nm)
0 %	35.43	100%	16.1135	15.23
	38.67	89%	14.5209	
	48.60	22%	15.0622	
0.2 %	35.50	100%	19.4567	17.41
	38.74	92%	15.6325	
	48.74	21.7%	17.1585	
0.4 %	35.50	100%	19.6107	17.44
	38.74	91.46%	15.5249	
	48.75	21.58%	17.2073	
0.6 %	35.50	100%	19.4563	17.49
	38.74	93%	15.5587	
	48.75	21,84%	17.4770	
0.8 %	35.50	100%	19.3986	17.51
	38.74	92.29%	15.6106	
	48.74	21.75%	17.5352	

The average crystallite size of CuO nanopowders doped with ZnO ranges from 15.23 nm to 17.51 nm. The increase in grain size with Zn doping can be explained by Vegard's law, where lattice distortion due to ionic radius differences causes the change in crystallite size (Mehraj et al., 2013). In the present system, the larger ionic radius of Zn^{2+} (0.74 Å) compared to Cu^{2+} (0.73 Å) leads to increased crystallite size when Zn^{2+} replaces Cu^{2+} in the CuO lattice structure (Mehraj et al., 2013).

C. FTIR Spectroscopy

Infrared analysis of the samples was carried out in transmission mode. Figures 8 and 9 show the transmission bands for unannealed CuO and CuO annealed at 450 °C, respectively. In Fig. 8, the unannealed CuO powder shows significant infrared absorption bands at wavenumbers 429.8 cm^{-1}, 497.6 cm^{-1}, and 603.7 cm^{-1}, which are specific to synthesized CuO powder (Ethiraj et al., 2012; O'Keeffe, 1963). Low-intensity absorption bands at 697.8 cm^{-1}, 751.6 cm^{-1}, and 859.6 cm^{-1}, as well as medium-intensity peaks at 1323.4 cm^{-1} and 1385.4 cm^{-1}, are attributed to acetic acid used in the synthesis. The band at 697.8 cm^{-1} corresponds to C–H deformation vibration, the band at 859.6 cm^{-1} corresponds to C–H bending vibration (McDevitt & Davidson, 1966), and the peaks at 1323.4 cm^{-1} and 1385.4 cm^{-1} correspond to C–H stretching vibration (Sullivan et al., 1992).

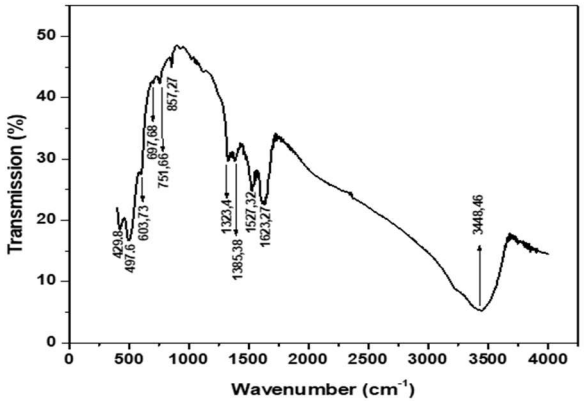

Figure 8 CuO infrared spectra without annealing

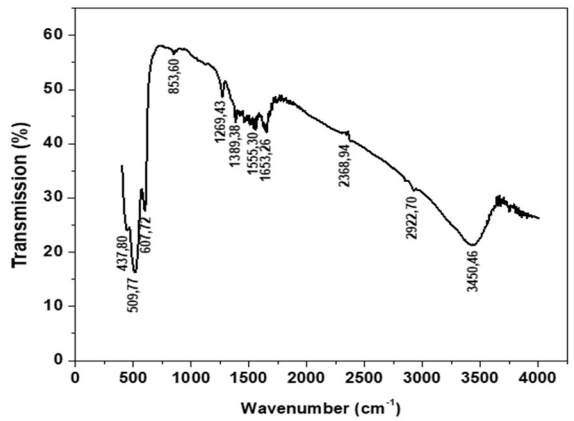

Figure 9 CuO infrared spectra at annealing temperature of 450°C

After annealing at 450 °C (Fig. 9), the absorption peaks at 697.8 cm^{-1} and 751.6 cm^{-1} disappeared, and the intensity of the peak at 859.6 cm^{-1} (C–H bending) drastically reduced. The absorption bands at 1623.2 cm^{-1} and 3448.4 cm^{-1} correspond to the deformation and stretching of the intermolecular O–H bond, respectively, due to the presence of water (H_2O). Following annealing at 450 °C, the absorption bands underwent a slight blue shift (shift toward shorter wavelengths).

D. Scanning Electron Microscopy

From the SEM images of the CuO samples (Figure 10), the powder exhibits a nanocluster form. The average crystallite dimensions obtained by the Scherrer formula are smaller than the grain dimensions observed by SEM, indicating that these grains are agglomerations of several crystallites.

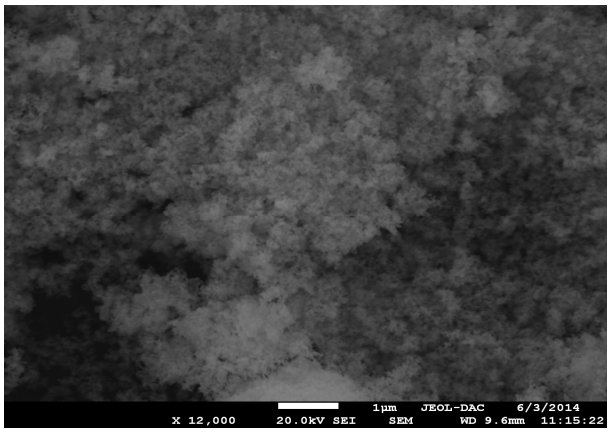

Fig. 10 SEM image of the CuO nano cluster

E. Optical Properties

1) UV-Visible Absorption

The absorption spectrum of the CuO film annealed at 450 °C is shown in Figure 11, and the second derivative of the absorption curve is shown in Figure 12. The variation of the absorption coefficient α with wavelength is presented in Fig. 11. The absorption coefficient decreases exponentially with increasing wavelength, a behavior typical of many semiconductors. Two absorption regions are observed: in the visible and near-UV region ($\lambda > 350$ nm), CuO absorbs nearly 33% of incident photons (transparent region); in the far-UV range ($\lambda < 350$ nm), CuO absorbs almost completely.

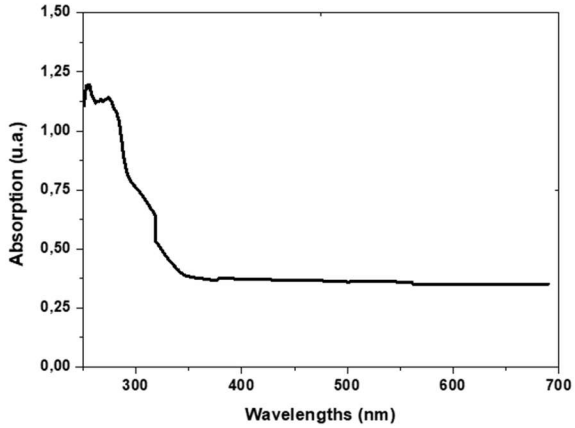

Figure 11 Absorption spectrum of CuO film at annealing temperature of 450 ° C.

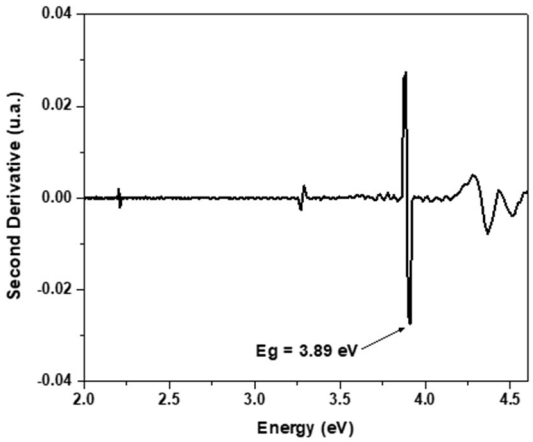

Figure 12 Gap of CuO of first technique deduced from the second derivative as a function of energy

2) Determination of the Optical Band Gap

(i) First method: Second derivative

The second derivative method was used to determine the optical band gap of CuO crystallites, as illustrated in Fig. 12. The obtained optical band gap value is 3.89 eV. Comparing this value to the band gap of bulk CuO (1.2 eV) reveals a blue shift of 2.7 eV. This shift is caused by quantum confinement of excitations, which occurs when crystallite size decreases to the nanometric scale, approaching the magnitude of the Bohr radius of the compound.

(ii) Second method: Tauc-Lorentz

The Tauc-Lorentz law is expressed by Equation 2:

$$(\alpha h\nu)^2 = A\,(h\nu - Eg) \quad (2)$$

The curve $(\alpha E)^2$ is plotted as a function of energy E for CuO thin films annealed at 450 °C, where α is the optical absorption coefficient and E is the energy of incident photons (E = hν). The direct optical band gap value is determined by extrapolating the linear portion of the $(\alpha h\nu)^2$ curve, as shown in Fig. 13. The intersection point with the horizontal axis gives the optical band gap value, which was determined to be 3.88 eV.

V. CONCLUSION

The objective of this study was to synthesize pure and ZnO-doped CuO nanopowders using the sol–gel precipitation method. Copper chloride dihydrate ($CuCl_2{\cdot}2H_2O$) was used as the precursor for pure CuO powders. This approach enabled the generation of a substantial amount of precipitate rapidly with basic equipment, allowing for an investigation into how heat treatment and doping influence the grain size and structure of the nanocrystallites. X-ray diffraction analysis revealed a monoclinic phase for all synthesized powders. An increase in annealing temperature correlated with the growth of crystallite size, which also expanded with higher doping percentages. For doped CuO/ZnO samples, the formation of CuO/ZnO nanocomposites was confirmed by the appearance of characteristic wurtzite ZnO peaks in the XRD patterns. The optical properties of the CuO/PMMA composite thin films permitted estimation of the optical band gap values, calculated to be approximately 3.88 eV and 3.89 eV using two different methods (Tauc-Lorentz and second derivative, respectively). The observed blue shift of ~2.7 eV relative to bulk CuO (1.2 eV) is attributed to quantum confinement effects due to the nanometric crystallite sizes (10.92–17.51 nm). In conclusion, the simple precipitation (sol–gel) method used in this work enables the preparation of well-crystallized CuO and CuO/ZnO nanopowders of good quality. These materials hold promise for future practical applications such as heterogeneous catalysis and optoelectronic devices.

Future work should extend the present findings by investigating intermediate ZnO doping concentrations (1–6%) and a broader range of annealing temperatures (200–850 °C) to optimize structural and optical properties. Photocatalytic activity testing using organic dye degradation under UV and visible light is recommended to evaluate environmental remediation potential. Additionally, gas sensing performance toward NO_2, H_2S, and humidity should be assessed. Electrical conductivity and magnetic property measurements would further clarify the role of Zn doping in charge transport and magnetic behavior. Comparative studies using hydrothermal or green synthesis methods may yield different morphologies with enhanced performance. Finally, scale-up synthesis and prototype device fabrication (solar cells, sensors, or photocatalytic reactors) are necessary steps toward practical applications.

AUTHOR CONTRIBUTIONS.

Bacha Rabie: Conceptualization, Methodology, Software, Validation, Writing – original draft, Writing – review & editing. **Chaieb and Bouchetout:** Supervision, Writing – original draft, Writing – review &editing.
Chala and Nuoi Y: Writing – review & editing.

ACKNOWLEDGEMENT(S)

The authors would like to thank Laboratory of crystallography, Physics Department, University of Constantine 1.and the Algerian General Directorate of Scientific Research and Technological Development (DGRSDT) for their scientific andacademic support.

REFERENCES

Agarwal, S., et al. (2019). Gas sensing properties of ZnO nanostructures (flowers/rods) synthesized by hydrothermal method. *Sensors and Actuators B: Chemical*, 292, 24–31. https://doi.org/10.1016/j.snb.2019.04.083.

Akpomie, K. G., Ghosh, S., Gryzenhout, M., & Conradie, J. (2021). One-pot synthesis of zinc oxide nanoparticles via chemical precipitation for bromophenol blue adsorption and the antifungal activity against filamentous fungi. *Scientific Reports*, 11(1), 1–17. https://doi.org/10.1038/s41598-021-87819-2.

Aldeen, T. S., Mohamed, H. E. A., & Maaza, M. (2020). Bio-inspired single phase Monteponite CdO nanoparticles via natural extract of Phoenix roebelenii palm leaves. *Journal of Inorganic and Organometallic Polymers and Materials*. https://doi.org/10.1007/s10904-020-01600-y.

Ashwani, S., Parveen, K., & Sanjay, D. (2017). Structural and optical study of Zn doped CuO nanoparticles synthesized by sol gel method. *Journal of Theoretical and Applied Sciences*, 9(5), 114–118.

Bandekar, S. S., et al. (2020). ZnO-CuO nanocomposites synthesis, characterization and antibacterial activity. *Journal of Physics: Conference Series*, 1706(1),

012018. https://doi.org/10.1088/1742-6596/1706/1/012018.

Cao, K., et al. (2019). CuO nanoplates for high-performance potassium-ion batteries. *Small*, 15(36), 1901775. https://doi.org/10.1002/smll.201901775.

Chala, S., et al. (2018). Extraction of ZnO thin film parameters for modeling a ZnO/Si solar cell. *Energy*, 164, 871–880. https://doi.org/10.1016/j.energy.2018.09.035.

Chala, S., et al. (2022). Dependence of structural and optical properties of ZnO thin films grown by sol–gel spin-coating technique on solution molarity. *Transactions on Electrical and Electronic Materials*. https://doi.org/10.1007/s42341-022-00386-9.

Chen, X., Wu, Z., Liu, D., & Gao, Z. (2017). Preparation of ZnO photocatalyst for the efficient and rapid photocatalytic degradation of azo dyes. *Nanoscale Research Letters*, 12(1), 4–13. https://doi.org/10.1186/s11671-017-1904-4.

Dasireddy, V. D. B. C., Rubin, K., Pohar, A., & Likozar, B. (2020). Surface structure–activity relationships of $Cu/ZnGaO_x$ catalysts in low temperature water–gas shift (WGS) reaction for production of hydrogen fuel. *Arabian Journal of Chemistry*, 13(4), 5060–5074. https://doi.org/10.1016/j.arabjc.2020.02.005.

Elbar, M., Tobbege, S., Chala, S., Saidani, O., Kateb, M. N., & Serdouk, M. R. (2023). Effect of temperature on the performance of CGS/CIGS tandem solar cell. *Journal of Nano and Electronic Physics*, 15(1), 1–6. https://doi.org/10.21272/jnep.15(1).01020.

Ethiraj, A. S., & Kang, D. J. (2012). Synthesis and characterization of CuO nanowires by a simple wet chemical method. *Nanoscale Research Letters*, 7(5), 1–5. https://doi.org/10.1186/1556-276X-7-70

García-Carrion, M., et al. (2020). Hybrid solar cells with β- and γ-gallium oxide nanoparticles. *Materials Letters*, 261, 127088. https://doi.org/10.1016/j.matlet.2019.127088.

Ghalmi, H., Bensmaine, L., Elbar, M., Chala, S., & Merzouk, S. (2022). Simulation study of CZTS/CZTSe tandem solar cell by using SCAPS-1D software. *Journal of Nano and Electronic Physics*, 14(6), 06033. https://doi.org/10.21272/jnep.14(6).06033

Jamali Sheini, F., Singh, J., Srivastava, O. N., Joag, D. S., & More, M. A. (2010). Electrochemical synthesis of Cu/ZnO nanocomposite films and their efficient field emission behaviour. *Applied Surface Science*, 256(7), 2110–2114. https://doi.org/10.1016/j.apsusc.2009.09.056.

Jan, T., et al. (2019). Superior antibacterial activity of ZnO-CuO nanocomposite synthesized by a chemical co-precipitation approach. *Microbial Pathogenesis*, 134, 103579. https://doi.org/10.1016/j.micpath.2019.103579

Jang, J. S., et al. (2019). Comparison study of ZnO-based quaternary TCO materials for photovoltaic application. *Journal of Alloys and Compounds*, 793, 499–504. https://doi.org/10.1016/j.jallcom.2019.04.042.

Kahsay, M. H. (2021). Synthesis and characterization of ZnO nanoparticles using aqueous extract of Becium grandiflorum for antimicrobial activity and adsorption of methylene blue. *Applied Water Science*, 11(2), 1–12. https://doi.org/10.1007/s13201-021-01373-w.

Kang, Y., Yu, F., Zhang, L., Wang, W., Chen, L., & Li, Y. (2021). Review of ZnO-based nanomaterials in gas sensors. *Solid State Ionics*, 360, 115544. https://doi.org/10.1016/j.ssi.2020.115544

Khadar, A. A. M. A. (2019). CuO–ZnO nanocomposite films with efficient interfacial charge transfer characteristics for optoelectronic applications. *SN Applied Sciences*, 1(9), 1–9. https://doi.org/10.1007/s42452-019-1002-6.

Kim, J. B., et al. (2008). Cu-doped ZnO-based p–n hetero-junction light emitting diode. *Semiconductor Science and Technology*, 23(9), 095004. https://doi.org/10.1088/0268-1242/23/9/095004.

Kumar, P., & Idem, R. (2007). A comparative study of copper-promoted water–gas-shift (WGS) catalysts. *Energy & Fuels*, 21(2), 522–529. https://doi.org/10.1021/ef060389x.

Lam, N. D. (2020). Modelling and numerical analysis of ZnO /CuO /Cu_2O heterojunction solar cell using SCAPS. *Engineering Research Express*, 2(2). https://doi.org/10.1088/2631-8695/ab9716.

Lavín, A., Sivasamy, R., Mosquera, E., & Morel, M. J. (2019). High proportion ZnO/CuO nanocomposites: Synthesis, structural and optical properties, and their photocatalytic behavior. *Surfaces and Interfaces*, 17, 100367. https://doi.org/10.1016/j.surfin.2019.100367.

Li, W. M., et al. (2019). Superconductivity in a unique type of copper oxide. *Proceedings of the National Academy of Sciences*, 116(25), 12156–12160. https://doi.org/10.1073/pnas.1900908116

Maache, M., Chala, A., & Devers, T. (2020). Characterization of spin coated tin oxide thin films for optoelectronic applications. *Journal of Nano and Electronic Physics*, 12(3), 1–5. https://doi.org/10.21272/jnep.12(3).03010

McDevitt, N. T., & Davidson, A. D. (1966). Infrared lattice spectra of cubic rare earth oxides in the region 700 to 50 cm^{-1}. *Journal of the Optical Society of America*, 56(5), 636–638. https://doi.org/10.1364/JOSA.56.000636.

Mehraj, S., Ansari, M. S., & Alimuddin. (2013). Structural, dielectric and complex impedance properties of Cd doped SnO_2 nanoparticles. *Journal of Nanoengineering and Nanomanufacturing*, 3(3), 229–236. https://doi.org/10.1166/jnan.2013.1137

Mursal, Irhamni, Bukhari, & Jalil, Z. (2018). Structural and optical properties of zinc oxide (ZnO) based thin films deposited by sol-gel spin coating method. *Journal of Physics: Conference Series*, 1116(3), 032020. https://doi.org/10.1088/1742-6596/1116/3/032020

Nikkhah, V., Sarafraz, M., & Hormozi, F. (2015). Application of spherical copper oxide (II) water nano-fluid as a potential coolant in a boiling annular heat exchanger. *Chemical and Biochemical Engineering Quarterly*, 29, 405–415. https://doi.org/10.15255/CABEQ.2014.2069

Noman, M. T., Amor, N., Petru, M., Mahmood, A., & Kejzlar, P. (2021). Photocatalytic behaviour of zinc oxide nanostructures on surface activation of polymeric fibres. *Polymers*, 13(8), 1227. https://doi.org/10.3390/polym13081227.

O'Keeffe, M. (1963). Infrared optical properties of cuprous oxide. *Journal of Chemical Physics*, 39(7), 1789–1793. https://doi.org/10.1063/1.1734530.

Parmigiani, F., & Samoggia, G. (1988). Experimental evidence of a fluctuating charge state in cupric oxide. *Europhysics Letters*, 7(6), 543–

548. https://doi.org/10.1209/0295-5075/7/6/011.

Qi, Q., Zhang, T., Zeng, Y., & Yang, H. (2009). Humidity sensing properties of KCl-doped Cu–Zn/CuO–ZnO nanoparticles. *Sensors and Actuators B: Chemical*, 137(1), 21–26. https://doi.org/10.1016/j.snb.2008.12.005.

Rahemi, S. A., Rouhaghdam, A. S., & Nazari, M. (2018). N-doped ZnO-CuO nanocomposite prepared by one-step ultrasonic spray pyrolysis and its photocatalytic activity. *Chemical Physics Letters*, 705, 19–22. https://doi.org/10.1016/j.cplett.2018.05.052.

Shaheera, M., et al. (2020). Characterization and device application of indium doped ZnO homojunction prepared by RF magnetron sputtering. *Optical Materials*, 101, 109723. https://doi.org/10.1016/j.optmat.2020.109723.

Sonker, R. K., Sabhajeet, S. R., Singh, S., & Yadav, B. C. (2015). Synthesis of ZnO nanopetals and its application as NO_2 gas sensor. *Materials Letters*, 152, 189–191. https://doi.org/10.1016/j.matlet.2015.03.112.

Sridar, R., Ramanane, U., & Rajesimman, M. (2018). ZnO nanoparticles synthesis, characterization and its application for phenol removal from synthetic and pharmaceutical industry wastewater. *Journal of Environmental Nanotechnology, Monitoring & Management*, 10, 388–393. https://doi.org/10.1016/j.enmm.2018.09.003.

Sukhorukov, Y., Loshkareva, N. N., Samokhvalov, A. A., Naumov, S. V., Moskvin, A. S., & Ovchinnikov, A. S. (1998). Magnetic phase transitions in optical spectrum of magnetic semiconductor CuO. *Journal of Magnetism and Magnetic Materials*, 183(3), 356–358. https://doi.org/10.1016/S0304-8853(97)01078-0.

Sullivan, D. H., Conner, W. C., & Harold, M. P. (1992). Surface analysis with FT-IR emission spectroscopy. *Applied Spectroscopy*, 46(5), 811–818. https://doi.org/10.1366/0003702924124844.

Swastika, T., Ardy, A., & Susanto, H. (2019). Preparation of catalyst Cu-ZnO-MgO-Al_2O_3 for direct synthesis of DME. *IOP Conference Series: Materials Science and Engineering*, 543(1), 012063. https://doi.org/10.1088/1757-899X/543/1/012063.

Taouririt, T. E., Meftah, A., Adaidak, N., & Chala, S. (2019). Effects of high-k gate dielectrics on the electrical performance and reliability of an amorphous indium–tin–zinc–oxide thin film transistor (a-ITZO TFT): An analytical survey. *Nanoscale*. https://doi.org/10.1039/C9NR03395E.

Thiwawong, T., Onlar, K., & Chaithanatkun, N. (2018). Preparation of copper doped zinc oxide nanoparticles by precipitation process for humidity sensing device. *AIP Conference Proceedings*, 2010, 020022. https://doi.org/10.1063/1.5053198.

Verrelli, R., Hassoun, J., Farkas, A., Jacob, T., & Scrosati, B. (2013). A new high performance CuO/$LiNi_{0.5}Mn_{1.5}O_4$ lithium-ion battery. *Journal of Materials Chemistry A*, 1(48), 15329–15333. https://doi.org/10.1039/C3TA13960C.

Wang, Y., et al. (2020). Solution-processed ITO thin-film transistors with doping of gallium oxide show high on-off ratios and work at 1 mV drain voltage. *Applied Physics Letters*, 116(14). https://doi.org/10.1063/1.5141140.

Wang, Z., et al. (2016). Magnetoelectric effect and phase transitions in CuO in external magnetic fields. *Nature Communications*, 7, 10295. https://doi.org/10.1038/ncomms10295.

Widiyandari, H., Umiati, N. A. K., & Dwi Herdianti, R. (2018). Synthesis and photocatalytic property of zinc oxide (ZnO) fine particle using flame spray pyrolysis method. *Journal of Physics: Conference Series*, 1025(1), 012004. https://doi.org/10.1088/1742-6596/1025/1/012004.

Xu, C., Manukyan, K. V., Adams, R. A., Pol, V. G., Chen, P., & Varma, A. (2019). One-step solution combustion synthesis of CuO/Cu_2O/C anode for long cycle life Li-ion batteries. *Carbon*, 142, 51–59. https://doi.org/10.1016/j.carbon.2018.10.016.

Yathisha, R. O., & Arthoba Nayaka, Y. (2018). Structural, optical and electrical properties of zinc incorporated copper oxide nanoparticles: Doping effect of Zn. *Journal of Materials Science*, 53(1), 678–691. https://doi.org/10.1007/s10853-017-1496-5.

Yip, S. K., & Sauls, J. A. (1992). Nonlinear Meissner effect in CuO superconductors. *Physical Review Letters*, 69(15), 2264–2267. https://doi.org/10.1103/PhysRevLett.69.2264.

Zhu, H., Han, D., Meng, Z., Wu, D., & Zhang, C. (2011). Preparation and thermal conductivity of CuO nanofluid via a wet chemical method. *Nanoscale Research Letters*, 6(1), 181. https://doi.org/10.1186/1556-276X-6-181.